available at www.sciencedirect.com

ScienceDirect

journal homepage: www.elsevier.com/locate/carbon

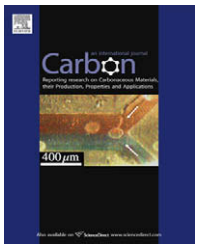

Diameter- and length-dependent self-organizations of multi-walled carbon nanotubes on spherical alumina microparticles

Delong He [a], *Michael Bozlar* [a,b], *Maxime Genestoux* [a], *Jinbo Bai* [a,*]

[a] *Laboratoire de Mécanique des Sols, Structures et Matériaux, Ecole Centrale Paris CNRS UMR8579, PRES UniverSud Paris, Grande Voie des Vignes, 92295 Châtenay-Malabry Cedex, France*

[b] *Laboratoire de Photophysique, Photochimie, Supramoléculaires et Macromoléculaires, Ecole Normale Supérieure de Cachan, CNRS UMR8531, PRES UniverSud Paris, 61 Avenue du Président Wilson, 94235 Cachan Cedex, France*

ARTICLE INFO

Article history:
Received 6 July 2009
Accepted 23 November 2009
Available online 26 November 2009

ABSTRACT

Multi-scale hybrid structures of multi-walled carbon nanotubes (MWCNTs) and micrometric alumina particles (μAl_2O_3) have been produced. The hybrid structures are obtained by in situ grafting carbon nanotubes (CNTs) on spherical μAl_2O_3 particles using an easy chemical vapor deposition method, without any pre-patterned catalyst treatment. The study of the influence of temperature and hydrogen ratio shows three regular hybrid structures defined according to CNT arrangement on μAl_2O_3. Furthermore, the organization modes demonstrate that the hybrid structures are strongly dependent on the diameter, length and area number density of CNTs. This dependency has been explained using a proposed nano-cantilever beam model. It evaluates the maximum deflection of one CNT due to weak van der Waals interactions. The model analysis shows that the MWCNT organizations are a result of varying competitive interactions between MWCNT rigidity and their attractive forces on the large curvature surface of μAl_2O_3. In addition, the influence of specific characteristics of μAl_2O_3 on hybrid structures is also discussed.

© 2009 Elsevier Ltd. All rights reserved.

1. Introduction

Carbon nanotubes (CNTs) have a wide range of applications from aerospace to electronics because of their extraordinary intrinsic mechanical, thermal, electrical properties and high aspect ratios [1–3]. Their hybridizations in polymer matrix with other materials, like nanosized metal or oxide particles, microsized ceramic particles, fullerenes and two dimensional graphene, exhibit superior multifunctional properties of polymer composites than pristine CNTs [4–8]. Meanwhile, to fully take advantage of such multi-scale combinations of CNTs with other nano or micrometric materials, it is required to have the essential connection between them, and especially the optimal CNT distribution and orientation in the matrix. Indeed, as previously reported, [4,9] CNTs are often in form of entangled aggregates and disorderly distributed in polymer matrix. Therefore, the development of more efficient hybridization ways and the control of CNT distribution and organization are two urgent issues, which need to be solved.

In situ grafting of CNTs on the surface of micrometric substrates using chemical vapor deposition (CVD) is an efficient way to produce nano–micro hybrid structures [10–12]. As largely reported about CNT growth on flat substrate, the diameter, length, area number density and organization of CNTs on micrometer-size particles depend on both substrate properties, including their size, morphology and their structure, and also on CVD synthesis parameters, such as carbon source, catalyst precursor, gas atmosphere, hydrogen ratio,

* *Corresponding author:* Fax: +33 1 41 13 1460.
E-mail address: jinbo.bai@ecp.fr (J. Bai).
0008-6223/$ - see front matter © 2009 Elsevier Ltd. All rights reserved.
doi:10.1016/j.carbon.2009.11.039

temperature, growth time, gas flow etc. The submicron SiO_2 spheres (diameter: ~0.5–1 μm) and CNT hybrid structures, reported by Huang [13], were obtained by pyrolyzing iron (II) phthalocyanine at 800–1000 °C. Then, isolated CNTs were perpendicularly grown on the surface of high curvature SiO_2 particles. Selective growth of aligned CNTs was obtained on the photolithographically patterned SiO_2 particles.

Nano–micro hybrid structures obtained by directly growing CNTs on micro SiC particles using CVD, demonstrated improved interfacial strength between the fillers and matrix in composites [11]. Large scale growth of vertically aligned CNT arrays on big diameter (~700 μm) ceramic spherical particles have been reported by Zhang et al. [14,15] and Xiang et al. [16] using ethylene or liquefied petroleum gas as carbon source, and ferrocene as catalyst precursor. It was also demonstrated that CNT arrays crack randomly into different bundles on the ceramic particles when the length of CNTs is above 400 μm. The growth of MWCNTs on alumina particles (volumetric diameter ~322 μm) supported iron catalyst powders were studied by Philippe et al. [17] in a fluidized bed-catalytic CVD, using ethylene as carbon source. The aligned MWCNT mats were first grown around the catalyst grains. Then entangled CNTs were formed from particles located inside the porosities of the support, with a fragmentation of the catalyst grains. In addition, hybrid structures of CNTs on ceramic fibers and carbon fibers have been produced by directly growing CNTs using CVD. Afterwards, these hybrid structures have been used to improve mechanical and thermal properties of composite materials [12,18–20].

However, the control of CNT organization and orientation in the hybrid structures has not been deeply investigated yet, especially in the case of micro ceramic particles without any pretreatment. But it is desirable to control CNT arrangements in the hybrid structures for achieving advanced multifunctional composite properties. The widely reported well-aligned CNT architectures, like the forms of arrays of CNT carpets, pillars, forests, etc.... [8,13,21–25], were generally obtained by exploring pre-patterned substrates or predefining catalyst nanoparticles into certain morphologies on the corresponding substrate. Then the selective decomposition of carbon sources resulted in different CNT patterns. It is worth mentioning that the pattern procedures are generally limited to be applicable to large flat surfaces. Obviously, these complex pretreatment techniques and strict application conditions greatly increase the difficulty and costs of elaborating aligned CNTs. Therefore, it is relevant to propose a facile CVD method to produce multiform hybrid architectures constituted of well-organized CNTs and micro ceramic particles without any pretreatment.

In this paper, we present multiform nano–micro hybrid structures of CNTs and micro-spherical alumina particles (μAl_2O_3). The well-organized hybrid structures are achieved by the self-organization of multi-walled carbon nanotubes (MWCNTs) on no pre-patterned μAl_2O_3 during CVD synthesis process. We find that the CNT organization on μAl_2O_3 is strongly dependent on their diameter, length and area number density. Three hybrid structures with distinct distribution patterns of CNTs and their evolution are demonstrated by changing CNT growth temperature, time and hydrogen ratio. The self-organization of the hybrids is explained by the CNT bending deflection caused by van der Waals interactions, using a CNT cantilever model.

2. Experimental

2.1. Sample preparation

The synthesis of CNTs was carried out by catalytic chemical vapor deposition (CVD) in a quartz tube (110 cm long, inner diameter 45 mm), which was heated to a given temperature (ranging from 450 to 900 °C) by a horizontal tube furnace (60 cm long) [19]. Micro-spherical alumina particles (μAl_2O_3, size ranging in 3–10 μm, with 99.8% purity including 800 ppm SiO_2, 600 ppm Na_2O), purchased from Performance Ceramic company (Peninsula, OH, USA), were used as substrate. One layer (~0.5 mm thick) of particles were first homogeneously dispersed on the surface of a quartz plate ($3 \times 50\ cm^2$), which was then put in the center of the furnace. The substrate was heated to the set temperature under the carrier gas argon and hydrogen (two flow rates were used: $1\ l\ min^{-1}$ and $0.8\ l\ min^{-1}$, with a varied hydrogen ratio.). Gas flows were accurately controlled by electronic mass flow meters (Bronkhorst, France). Ferrocene ($Fe(C_5H_5)_2$, concentrated at $0.05\ g\ ml^{-1}$) was dissolved in xylene (C_8H_{10}) to serve as catalyst precursor. Then, the mixture was fed by a syringe system (at a rate of $\sim 0.2\ ml\ min^{-1}$) and carried into the preheated stable reaction zone in the form of spray by carrier gas. In particular, acetylene ($10\ ml\ min^{-1}$) was injected when hydrogen ratio was changed at 550 °C. In general, the CNT growth time was 15 min. At the end, the furnace was cooled down under argon and hydrogen atmosphere ($1\ l\ min^{-1}$).

2.2. Characterization

The collected samples were characterized by the following techniques: scanning electron microscope (SEM, LEO Gemini 1530), transmission electron microscope (TEM, Jeol 1200 EX), high resolution transmission electron microscope (HRTEM, Philips CM20-UT), Raman spectrometer (Jobin Yvon), X-ray diffraction (Siemens D5000, Cu Kα radiation (λ = 1.54069 Å)).

3. Results and discussion

The general formation mechanisms of the hybrid structures consist in two steps. First, nanoscale catalyst particles are formed on micro alumina substrate by the decomposition of ferrocene. In a second step, the formed catalyst particles generate MWCNT nucleation and growth. Therefore, this ensures that CNTs are connected to μAl_2O_3 along their axial direction, which is essential to build efficient charge and load transfer interfaces. Here, pristine spherical μAl_2O_3 particles with no pretreatment are chosen as substrate for the following reasons. First, alumina is an efficient substrate for CNT growth in CVD process. Second, the big curvature ($\sim 10^6\ rad\ m^{-1}$) and symmetric geometry of μAl_2O_3 promote the CNT dispersion. Finally, its excellent thermal conductivity, dielectric properties, wear-resistance and high temperature stability favor it to develop advanced multifunctional hybrid structures

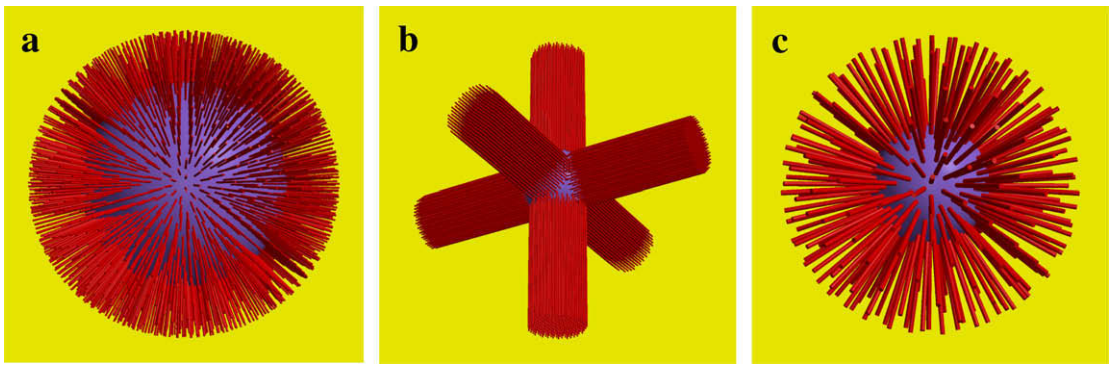

Fig. 1 – Schematic of three distinct MWCNT–μAl_2O_3 hybrid structures due to different CNT distribution patterns. (a) "Short-dense-homogeneous": highly dense and vertically aligned short CNTs homogeneously cover the whole surface of μAl_2O_3; (b) "six-branch": CNTs in independent branches are uniformly distributed in six-directions. (c) "Urchin-like": low area number density and long CNTs get out from μAl_2O_3 like the spines of sea urchin.

for a variety of applications. Three resulting distinct hybrid structures are schematically described as follows: "short-dense-homogeneous", "six-branch", and "urchin-like" (Fig. 1). This classification is based on CNT diameter, length, area number density and their organization states. As shown in the schematic, the consecutive structure transformation from "short-dense-homogeneous" to "urchin-like" is like flowering process in nature. These transformations are greatly dependent on CNT diameter and length, which are modulated by just changing hydrogen ratio and temperature in the CVD process.

3.1. *Influence of the CNT length on the hybrid organization*

Fig. 2 shows different CNT organizations on μAl_2O_3 and their consecutive transformation with increasing CNT length and aspect ratio (*L*/*D*, length/diameter). The aspect ratio was changed by adjusting hydrogen ratio in the total carrier gas flow (1 l min^{-1}). Hydrogen flow varied from 0.4 to 0 l min^{-1} in series of 0.4, 0.2, 0.1, 0.05 and 0 l min^{-1}. The synthesis temperature of CNTs was 550 °C. In particular, acetylene was fed at 10 ml min^{-1} simultaneously with the xylene solution. At this temperature, only few amount of xylene is decomposed, simply because it has a high decomposition temperature. Therefore, in this case, xylene served mainly as a solvent for dissolving catalyst precursor. Then the dissolved solution was then injected in form of spray into the CVD furnace by a syringe. In this way, it is much easier to control the carbon/iron ratio for the growth of CNTs. However, acetylene is here the major carbon source for CNT growth, and it has much higher decomposition rates, even at low temperatures [26–28]. This is clearly seen through the analysis of SEM images corresponding to hybrid structures obtained at 550 °C, using in the first case a mixture of xylene and acetylene as carbon source, and in the second one, only xylene.

Hydrogen plays an important role in controlling the CNT length, and particularly in influencing the decomposition of catalyst precursors and carbon sources [29]. Additionally, it avoids the formation of amorphous carbon on the surface of iron catalysts and thereby promotes the effective lifetime of the catalyst [30,31]. As shown in Fig. 2h, CNT average length decreases gradually while the hydrogen ratio increases. However, its diameter in different organization patterns is always about 10 nm (Fig. 2g). Thereby the CNT aspect ratio and length decrease simultaneously with increasing the hydrogen ratio (Fig. 2h). It is found that the CNT organization pattern changes progressively from short homogenous state to six equally separated branches on the surface of μAl_2O_3, with increasing the aspect ratio.

In Fig. 2a, CNTs are organized in "short-dense-homogenous" patterns when their length is 1 μm and their aspect ratio 100. Scanning electron microscopy (SEM) and transmission electron microscopy (TEM) characterizations display homogenously and vertically aligned CNTs on the surface of the alumina substrate. Such hybrid structures are obtained when hydrogen ratio is 40 vol.%. However, at the same hydrogen level, the whole continuous CNT layer gradually splits into six equal parts when the aspect ratio is 120 (Fig. 2b). The decrease of hydrogen ratio (20%, 10% and 5%) yields to an increase of the CNT average length, and further to an augmentation of aspect ratio (~150 when H_2 = 20% (Fig. 2c); ~350 when H_2 = 10% (Fig. 2d) and ~450 when H_2 = 5% (Fig. 2e)). The lower is hydrogen ratio, bigger is the CNT aspect ratio, and finally the more evident is the "six-branch" morphology. In the absence of hydrogen, six thinner and longer CNT branches grow at the six poles of the spherical alumina microparticle, as shown in Fig. 2f. This is explained by the fact that the decompositions of both catalyst precursor and carbon source are accelerated when hydrogen is removed from the reaction system. Whereas, a supplementary contribution of μAl_2O_3 substrate to CNT growth is limited.

The change of MWCNT organization from low to high aspect ratio lets us thinking about a natural flowering process. During this process from "short-dense-homogenous" to "six-branch", the CNT diameter and area number density keep nearly the same value, except in the absence of hydrogen. Therefore, in this case, the increases of CNT length and aspect ratio are the main factors responsible for their organization on the μAl_2O_3 particles.

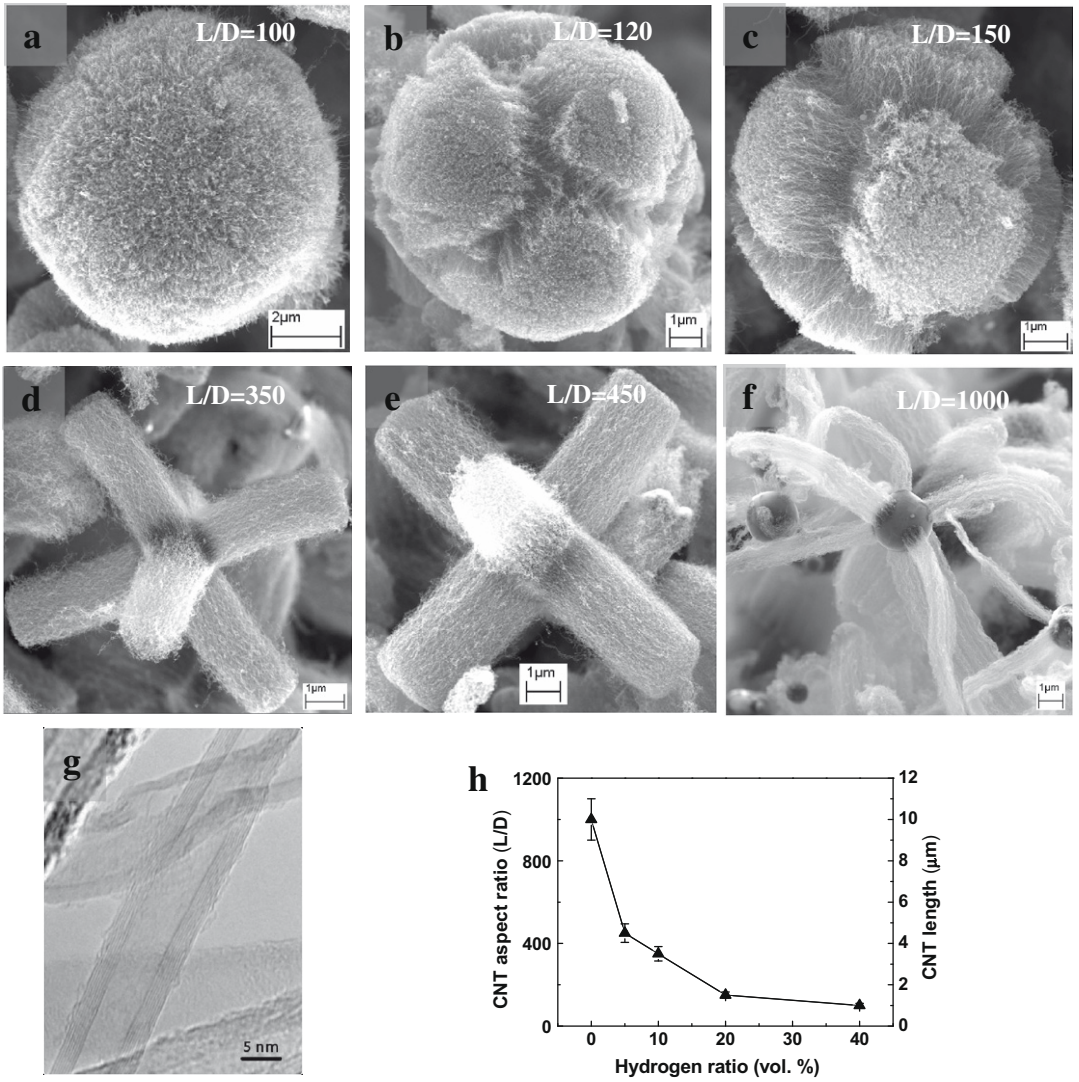

Fig. 2 – SEM images of self-organized CNT patterns on μAl_2O_3 with different aspect ratios (*L/D*). The hybrid organization changes from "short-dense-homogenous" to "six-branch" when the hydrogen ratio decreases from 40% to 0%. (a) *L/D* = 100 when 40% H_2; (b) *L/D* = 120 when 40% H_2; (c) *L/D* = 150 when 20% H_2; (d) *L/D* = 350 when 10% H_2; (e) *L/D* = 450 when 5% H_2; and (f) *L/D* = 1000 when no H_2. (g) High resolution TEM image of CNTs obtained when hydrogen ratio is 10%. (h) The curve represents the evolution of CNT length and aspect ratio with decreasing hydrogen ratio.

3.2. *Influence of the CNT diameter and area number density on the hybrid organization*

Fig. 3 shows the different CNT organizations on μAl_2O_3 and the corresponding consecutive transformations from "six-branch" to "urchin-like" states, while the CNT diameter increases. These hybrid structures were prepared using xylene as carbon source at temperatures ranging from 550 to 800 °C. The total gas flow rate was fixed to 0.8 l min^{-1}, in which hydrogen and argon flow rates were fixed at 0.08 l min^{-1} and 0.72 l min^{-1}, respectively. Highly dense MWCNTs grown in six different parts are vertically aligned on the μAl_2O_3 at 550 °C (Fig. 3a), and their diameters and lengths are ~10 nm and 1 μm, respectively. When CNT diameters are around 10 nm (600 °C) or 15 nm (650 °C), they are always configured in "six-branch" (Fig. 3b and c). However, the "six-branch" structures become less evident when CNT average diameters are ~20 nm at 700 °C (Fig. 3d). Beyond this temperature, the chemical decomposition of ferrocene and xylene is intensified. Finally, both the average diameter and length increase continuously with the temperature, while the area number density decreases.

As a result, the "urchin-like" hybrid architecture appears at 750 and 800 °C (Fig. 3e–f). The CNT diameters have a considerable augmentation and vary in a large region at these temperatures. Indeed, SEM and TEM observations confirm a decrease of CNT area number density on the surface of μAl_2O_3. The influence of the temperature on MWCNT diameter, length and aspect ratio is shown in Fig. 3h. Both diameter and length of CNTs increase continuously with the temperature, and even drastically after 700 °C. Whereas, the CNT aspect ratio in these cases fluctuates in a narrow range,

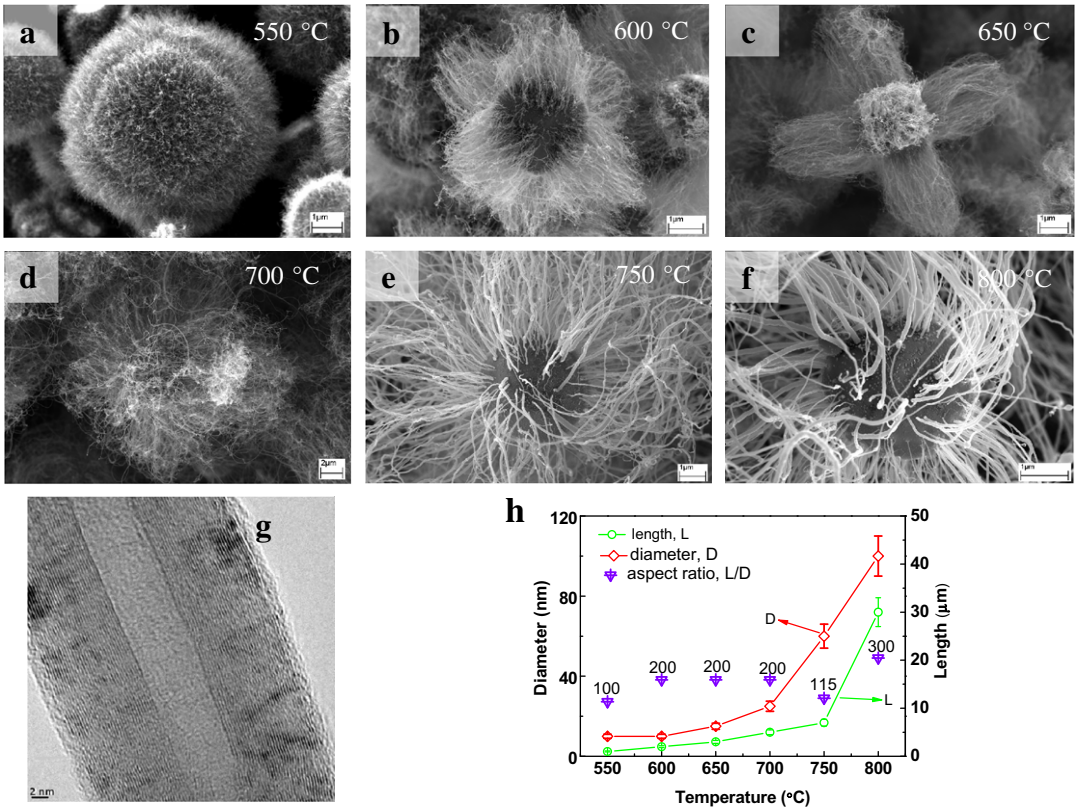

Fig. 3 – SEM images of the self-organized CNT patterns on μAl_2O_3 obtained at different temperatures. The diameter and length were modulated by increasing the synthesis temperature from 550 to 800 °C with a step of 50 °C, as chronologically represented in images (a–f). (g) High resolution TEM image of one CNT obtained at 750 °C. (h) Temperature dependence of the average diameter and length of CNTs and the corresponding aspect ratio.

especially from 100 to 300. At this point, it is worth to mention that the diameter variations contribute more than the length to the hybrid structuration.

It is worth noticing that CNT diameter is generally related to the area number density of CNTs on the surface of particles in the catalytic CVD process. This could be previously seen in Figs. 2 and 3. CNTs with small diameters have normally higher area number density than those with big diameters. The high CNT growth temperature promotes normally the formation of "urchin-like" structures with lower area number density of CNTs when xylene is used as carbon source.

Sometimes, "urchin-like" hybrid structures with high area number density of CNTs could also be seen even at high temperature, especially for particles located in the front part of the quartz plate. In this area, near the injection zone of carrier gases and carbon source–catalyst precursor solution, higher density catalyst precursors and their decomposed fragments are present. In addition, this zone contains high concentration of decomposed carbon sources promoting CNT growth. Consequently, CNTs with high area number density on micro alumina spheres are formed, as shown in Fig. 4a and b. As it is shown, CNTs with high area number density have still "urchin-like" structures, as in the case of low area number density. This is different than the previous cases (Figs. 2 and 3), where the high area number density of CNTs generates preferentially "six-branch" structures at low synthesis temperature. Such "urchin-like" structures show that big diameter CNTs, obtained at high temperature maintain their vertical alignment on the surface of μAl_2O_3, even at high area number density. This confirms that the diameter contributes more than the area number density to the self-organization of the hybrids.

3.3. *Raman spectroscopy of the three hybrid structures*

Hybrid structures were characterized by Raman spectroscopy in order to understand their chemical structures and homogeneity. Raman spectra corresponding to the three different hybrid structures and pristine spherical alumina are plotted in Fig. 5. In the case of "six-branch" and "urchin-like" structures, the common evident peaks related to alumina are visible around 220, 286 and 408 cm^{-1}, and two slight ones at 610 and 730 cm^{-1}. But the peaks relative intensity ratios differ for these two types of structures.

Furthermore, one significant peak (252 cm^{-1}) for "urchin-like" structures disappears in the spectrum of "six-branch" structure. But for "short-dense homogeneous" structure, Raman peaks between 200 and 900 cm^{-1} are not visible. This can be attributed to the different CNT coverage levels on alumina surface which influence the accessibility of the excitation laser. Indeed, high area number density CNTs recover almost the entire surface of the ceramic particles, and thus, no evident signals are detected for the "short-dense-homogeneous" structure.

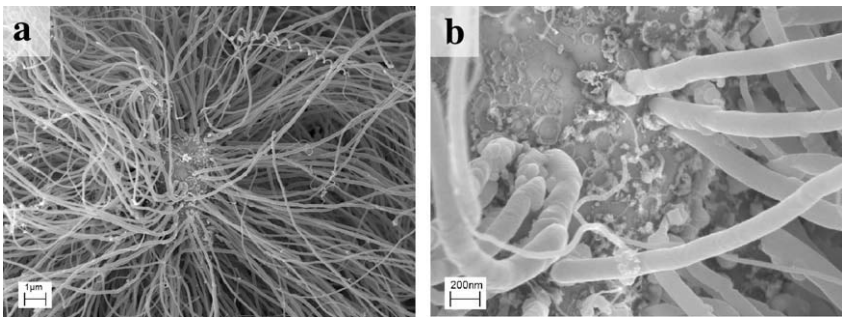

Fig. 4 – "Urchin-like" hybrid structures with high CNT area number density on micro alumina particles. The synthesis was conducted at 800 °C using xylene as carbon source. The solution (ferrocene dissolved in xylene with a concentration of 0.1 g ml^{-1}) was injected into the furnace at 0.2 ml min^{-1} for 15 min. (a) High CNT area number density: collected from the front of quartz plate (~20 cm before the middle part); (b) high magnification SEM of image (a).

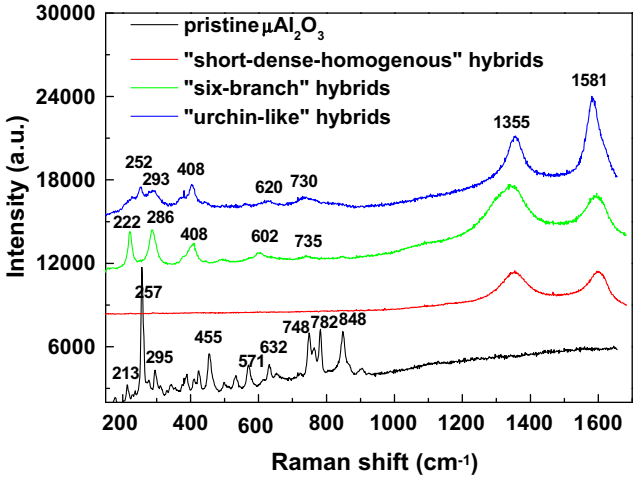

Fig. 5 – Raman spectra of pristine μAl_2O_3 and hybrid structures with three different morphologies. The spectra were obtained at room temperature using an excitation wavelength of 514.5 nm. The legend indicates: pristine μAl_2O_3 powders without any treatment and decomposition of carbon; "short-dense-homogeneous" hybrid structures (shown in Fig. 2a) produced at 550 °C using 0.4 l min^{-1} H_2 and 10 ml min^{-1} C_2H_2; "six-branch" hybrid structures (shown in Fig. 2d) produced at 550 °C using 0.1 l min^{-1} H_2 and 10 ml min^{-1} C_2H_2; "urchin-like" hybrid structures (shown in Fig. 3e) produced at 750 °C using 0.1 l min^{-1} H_2 and 0.05 g ml^{-1} ferrocene in xylene.

Then, the disorder-induced *D*-band (sp^2-hybridized carbon materials) is clearly visible at 1350 cm^{-1} in all three cases. The graphite-like *G* band corresponding to in-plane tangential mode of two carbon atoms in a graphene unit cell is identified around 1581 cm^{-1} [1]. Graphitization rate of CNTs in hybrid structures could be evaluated by the half width at half-maximum of *G* band, the intensity of *D*-band and the relative intensity ratio (I_D/I_G) [32]. A general comparison of the characteristic peaks of CNTs shows that "urchin-like" structures have the highest graphitization rate, in terms of sharper peaks at 1350 and 1580 cm^{-1} and the smallest intensity ratio I_D/I_G.

3.4. *Influence of CNT growth time on the hybrid organization*

The evolution of MWCNT–μAl_2O_3 hybrids at different growth times has been shown in Fig. 6. The hybrids were produced using acetylene (0.01 l min^{-1}) and xylene (at an injection rate of ~0.2 ml min^{-1}) as carbon source at 600 °C. The carrier gas flow rate is 1 l min^{-1} including 30% hydrogen and 70% argon. The hybrids with different CNT synthesis times were analyzed. It is found that under the selected conditions the hybrids have always the "six-branch" structure from a short CNT growth time (2 min) to a larger one (20 min). The length of CNT branches progressively augments in a quasi linear manner with the growth time, which is similar to the case reported by Zhang et al. [14] and Xiang et al. [16]. Consequently, the vertically aligned branches with short length (Fig. 6, at 2 min) grew gradually into the curved ones with irregular wave shapes (Fig. 6, at 20 min) due to the surrounding neighbor particles when the CNT length increases. At the same time CNT branches are more sensitive to deformation. However, it should be noticed that there is no evident change of the CNT area number density at different growth times.

3.5. *Mechanism discussion for the formation of multiform MWCNT–μAl_2O_3 hybrids*

The precedent analyses have in fact involved three configurations of MWCNT–μAl_2O_3 hybrids and their transformation processes, as schematically given in Fig. 1. It has been shown that the variations of the diameter, length and CNT area number density play a key role in the final morphologies. Besides, the hybrid structures, especially "six-branch" ones, are also related to the special characteristics of the morphology and structure of μAl_2O_3. In order to understand deeply the formation mechanism of the hybrids, the following parts give more detailed discussions, which are developed around two significant aspects: μAl_2O_3 crystallography and CNT self-organization behavior.

3.5.1. *Micro alumina particles crystallography*

As shown in Fig. 2, homogenously and vertically aligned CNTs on the surface of μAl_2O_3 will crack or break into different bun-

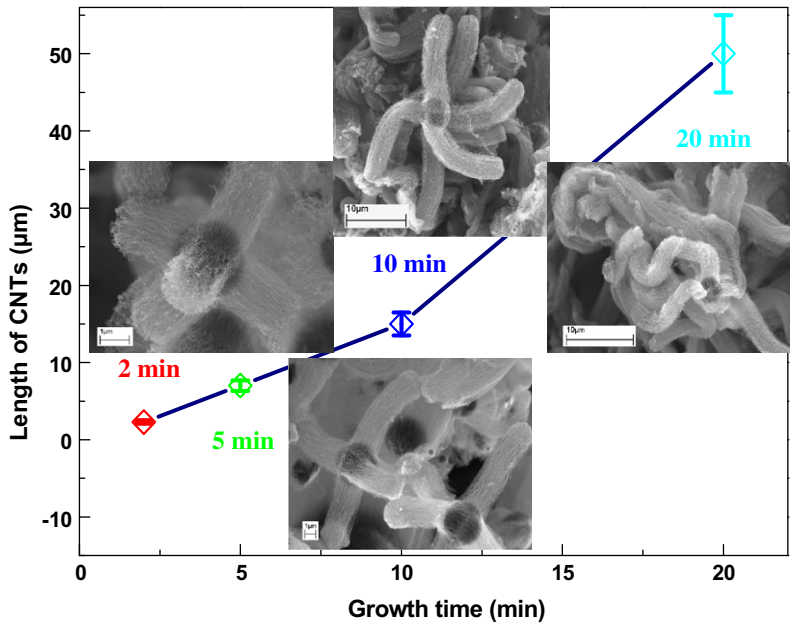

Fig. 6 – Evolution of the morphologies of MWCNT–μAl_2O_3 hybrids with growth time. The CNT growth was conducted at 600 °C using 30 vol.% hydrogen, at different times: 2, 5, 10 and 20 min.

dles when their length is larger than 1 μm. Similar phenomenon was also reported in the cases using fibers and other spherical ceramic particles as substrate when CNT lengths exceed one critical value. However, in our case, large quantities of regular "six-branch" structures are formed rather than, random and irregular bundles, as reported elsewhere [14,16,17]. Moreover, the same "six-branch" hybrid structures appear even though the experiment conditions are changed. It was also found that the starting point of the self-assembly is located at the six polar zones of the μAl_2O_3. Then it expands to broader region when changing the synthesis conditions, and finally it is limited to 12 lines, which form an inscribed cube in the micro sphere, as displayed in Fig. 7a. The cubic morphology is clearly seen from the distribution of MWCNTs, which are obtained at 450 and 550 °C by the addition of C_2H_2 during 15 min (Fig. 7b and c).

The cubic boundary for the "six-branch" hybrid structures may derive from the crystallographic characteristics of the micro substrate. The spherical alumina particles were fabricated by melting in a plasma flame irregular alumina particles, which were previously sized and fused. Afterwards, the molten droplets of Al_2O_3 were formed in spherical shapes due to surface-tension effects. As previously reported [33], the alumina particles produced by this way exhibit differences in crystallography because of different cooling rates in one particle.

X-ray diffraction spectrum (Fig. 8) shows that they contain not only thermodynamically stable hexagonal α-Al_2O_3, which

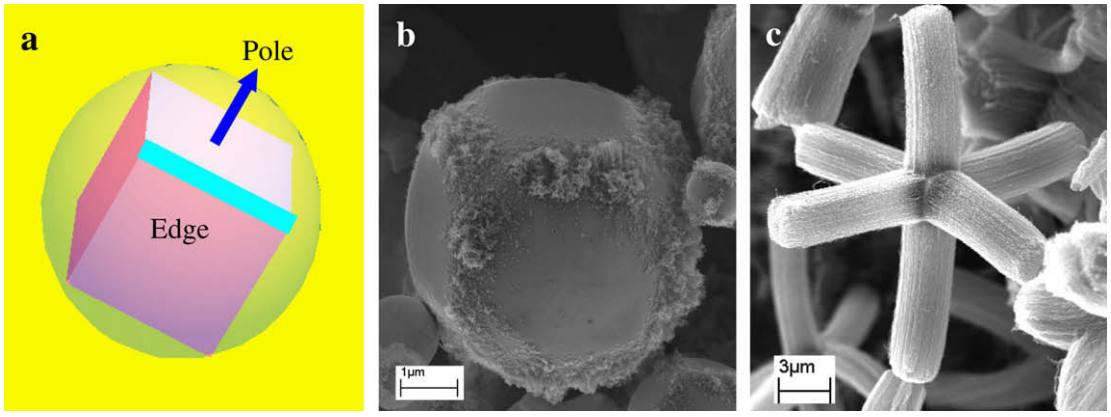

Fig. 7 – (a) Schematic representing the spherical alumina particle containing 6 poles and 12 edges. (b) SEM image of μAl_2O_3 spherical particles after exposing in C_2H_2 (10 ml min^{-1}) during 15 min at 450 °C. The regions of MWCNT growth is like the 12 edges of the cube inscribed in the micro sphere alumina. (c) MWCNTs organized in "six-branch" on the surface of μAl_2O_3 particles with C_2H_2 (40 ml min^{-1}) at 550 °C during 15 min. The total flow rate of carrier gas was 1 l min^{-1} and the concentration of ferrocene in xylene was 0.05 g ml^{-1}.

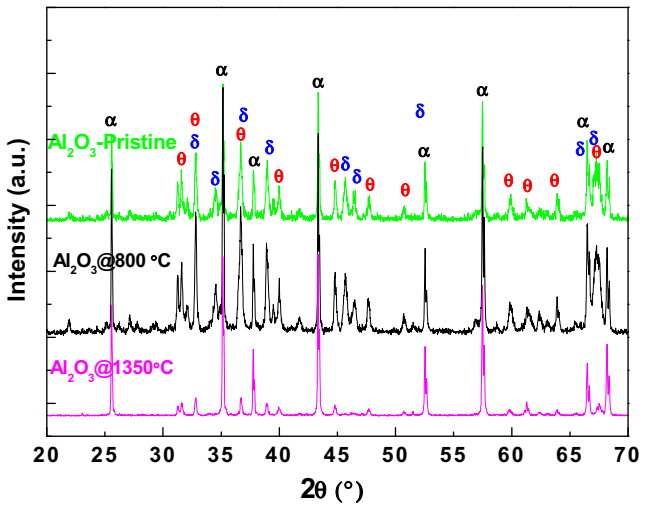

Fig. 8 – X-ray diffraction spectra of pristine micro alumina spherical particles before grafting MWCNTs on their surface. For comparison, the particles have been heated at 800 and 1350 °C during 4 h.

is the predominant phase, but also metastable tetragonal δ and monoclinic θ phases. Generally, the structure of δ- and θ-Al_2O_3 is located within the surface layer due to the rapid quench speed during the solidification of particles, but α-Al_2O_3 inside the particles [34]. This is also proven by the Raman spectrum of pristine particles (Fig. 5). The α-Al_2O_3 characteristic peaks at 418 and 645 cm^{-1} for A_{1g} modes and at 378, 433, 451, 578 and 751 cm^{-1} for E_g modes are invisible in the spectrum [35]. Whereas, the intensities of Raman shift between 200 and 900 cm^{-1}, associated to δ- and θ-Al_2O_3, are more evident.

The six evident peaks are present at the positions around 257, 455, 632, 748, 782 and 848 cm^{-1}. It indicates that the predominant α-Al_2O_3 is surrounded inside the sphere by a layer of δ- and θ-Al_2O_3 structure, so that only small amount of α-Al_2O_3 can be accessed by the laser source. The X-ray spectrum corresponding to μAl_2O_3 particles at 800 °C reveals that no phase-transformations have occurred in comparison with the spectrum of pristine μAl_2O_3. Meanwhile, these metastable phases could occur certain structural transformation after moderate heat treatment, and transform completely to α-Al_2O_3 when the heat treatment temperature is higher than 1473 K (Fig. 8) [34]. This specific structure could be the origin of an inherent inscribed cube and potentially cause heterogeneous nucleation and growth of CNTs on the μAl_2O_3 surface. More detailed influences of the μAl_2O_3 particles crystallographic structures on the CNT organization mechanisms are still under research. However, these differences can be relatively intensified or weakened according to synthesis condition during MWCNT growth.

3.5.2. *CNT self-organization model*

It is noticed that each of the three hybrid structures possesses specific CNT diameter, length and area number density on μAl_2O_3. It is desirable to propose an appropriate model, which could globally describe the relationship between CNT diameter, length, area number density and in consequence the hybrid structure organizations. In the following parts, we use a CNT nano-cantilever model to analyze the deflection of a single CNT in two positions: from vertically aligned to parallel with the neighbor CNTs, as shown in Fig. 9a. This model is based on the analysis of the weak van der Waals interaction (vdW) forces between two CNTs which promote individual CNTs to form bundles.

Indeed, vdW forces exist extensively in CNT growth process and remain in the obtained materials. For instance, vdW forces contribute largely to the self-assembly of single-walled CNTs into bundles, and also to the self-folding of one CNT into racket-structures [36–39]. Another significant effect of vdW forces is the formation of high area number density vertically aligned single-walled or MWCNT arrays which are normally produced on flat substrate by CVD method [23,40,41]. As previously indicated, the exceptional mechanical properties, especially high Young's modulus (~1 TPa) [2,3], ensure short CNTs high stiffness to resist to the bending deformation, and to grow perpendicularly to the surface of the substrate.

In the case of "short-dense-homogenous" and "urchin-like" hybrid structures, CNTs grow vertically to the surface of spherical particles. Meanwhile, in "six-branch" structures, CNTs self-assemble into bundle structures, where parallel CNTs are only aligned along six-directions due to their own deflection. And this deflection of CNTs results from the interaction between vdW forces and the resistance to bending caused by their high rigidity.

The continuum Lennard–Jones (LJ) model is widely used to evaluate the vdW potential energy of interactions in any types of graphitic structures, including CNTs [36,39,42]. It was found that the interaction potentials between two arbitrary CNTs have the same curve when plotted in terms of certain reduced parameters, the well depth $\phi(R_0)$, and equilibrium vdW gap $(R_0 - \rho)$, which is from 3.107 to 3.169 Å [36,42,43]. As Sun suggested, $R_0 - \rho$ has a given value of 3.15 Å. R_0 is the equilibrium spacing at the minimum energy for the two interacting entities; ρ corresponds to the sum of the radii of two interacting CNTs. The potential of two parallel and infinitely long single-walled CNTs can be represented by a simple analytical form as suggested by Girifalco et al. [36] and Sun et al. [42], as follows:

$$\widetilde{\phi}(\widetilde{R}) = -\frac{1}{0.6}\left[\left(\frac{3.41}{3.15\widetilde{R}+0.28}\right)^4 - 0.4\left(\frac{3.41}{3.15\widetilde{R}+0.28}\right)^{10}\right], \quad (1)$$

where $\widetilde{\phi}(\widetilde{R}) = \frac{\phi(R)}{|\phi(R_0)|}$, $\widetilde{R} = \frac{(R-\rho)}{(R_0-\rho)}$, $\phi(R)$ is the potential energy of interaction per unit length, and R is the perpendicular distance between CNT centers, which could be written as:

$$R = \widetilde{R}(R_0 - \rho) + \rho. \quad (2)$$

Therefore, the interaction potential between two MWCNTs could be written as:

$$\phi^{AB}(R) = -\frac{|\phi(R_0)|}{0.6}\left(\left(\frac{3.41}{R-\rho+0.28}\right)^4 - 0.4\left(\frac{3.41}{R-\rho+0.28}\right)^{10}\right). \quad (3)$$

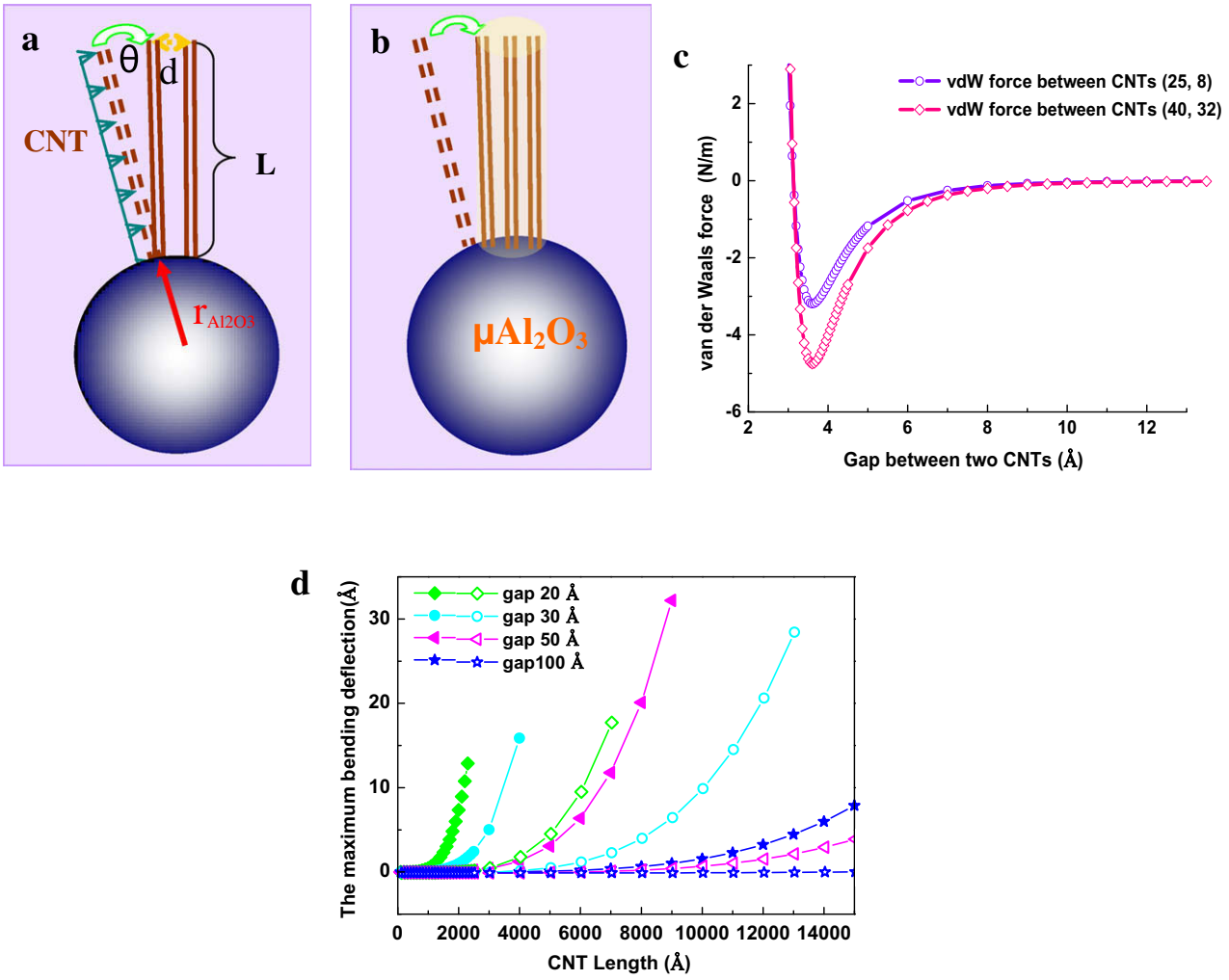

Fig. 9 – Weak interactions between CNTs and nano-cantilever model to analyze the agglomeration of CNTs on μAl_2O_3. (a) Schematic of the interaction (uniform distribution loading) of two adjacent CNTs: perpendicularly grown CNTs (*L*, length) are seen as nano-cantilevers with one end fixed to the surface of μAl_2O_3, with radius r_{Al2O3}. The gap between two CNTs at the root is noted with *d*. θ corresponds to the angle resulting from the deflection of one CNT. (b) Schematic of the initial agglomeration of CNTs into bundles at one pole of alumina particle due to the weak vdW interactions; (c) curves of vdW forces between two pairs of parallel MWCNTs indicated by CNT(25, 8)–(25, 8) and CNT(40, 32)–(40, 32), according to Girifalco et al. [36] and Sun et al. [42] proposed model; (d) relationships between the maximum deflections of CNTs(25, 8)–(25,8) and (40, 32)–(40, 32), and their lengths, when CNT gaps are 20, 30, 50 and 100 Å, respectively. Solid and hollow symbols indicate CNT(25, 8) and CNT(40, 32), respectively.

At this point, the problem is transferred to how to obtain the value of $\phi(R_0)$.

Here, we use the method proposed by Sun et al. [42,43] to evaluate approximately the potential expression. Two MWCNTs *A* and *B* interaction are expressed by an index $(r^A_{inner}, n_A) - (r^B_{inner}, n_B)$ in the continuum model. r^A_{inner} and r^B_{inner} indicate the inner radii for tubes *A* and *B*, respectively. n_A and n_B stand for the number of layers in tubes *A* and *B*, respectively. The interlayer spacing is assumed constant, $c = 3.39$ Å. The potential energy (ϕ^{AB}) for $(r^A_{inner}, n_A) - (r^B_{inner}, n_B)$ was calculated by summarizing all the interactions (ϕ^{ij}) between the *i* layer of tube *A* and the *j* layer of tube *B*, here $i = 1, 2, \ldots, n_A$ and $j = 1, 2, \ldots, n_B$. As proposed by Sun et al. [43], the well depth of two MWCNTs ϕ_0^{AB} could be approximately estimated by:

$$\phi_0^{AB} = \phi_0^{n_A n_B} + 0.13\left(\phi_0^{(n_A-1)n_B} + \phi_0^{n_A(n_B-1)}\right) + 0.03(\phi_0^{(n_A-2)n_B} + \phi_0^{(n_A-1)(n_B-1)} + \phi_0^{n_A(n_B-2)}) + 0.01(\phi_0^{(n_A-3)n_B} + \phi_0^{(n_A-2)(n_B-1)} + \phi_0^{(n_A-1)(n_B-2)} + \phi_0^{n_A(n_B-3)}) \quad (4a)$$

$$\text{where} \quad \phi_0^{ij} = -\sqrt{\left(3.13 - 37.9\sqrt{R_i^A}\right) \times \left(3.13 - 37.9\sqrt{R_j^B}\right)} \quad (4b)$$

$$R_i^t = R^t_{inner} + (i-1) \times c \quad (i = n_t, \ldots, n_{t-3}; \quad t = A, B) \quad (4c)$$

Potential terms (ϕ_0^{AB} and ϕ_0^{ij}) and radii (R_i^t and R^t_{inner}) are in units of meV/Å and Å, respectively.

In our case, CNT diameter is homogeneous in "short-dense-homogeneous" and "six-branch" hybrid structures. According to HRTEM observations, its inner radius is ~25 Å, and one CNT contains eight layers. It is therefore reasonable to assume all the CNTs with the same index, in the form (r_{in}-

ner, 8). Then, we calculate using Eq. (4) the potential between any pair of CNTs $\phi_0^{AB} = -360.72$ meV. Furthermore, the potential ϕ^{AB} could be finally expressed by:

$$\phi^{AB}(R) = -\frac{360.72}{0.6}\left(\left(\frac{3.41}{R-50+0.28}\right)^4 - 0.4\left(\frac{3.41}{R-50+0.28}\right)^{10}\right). \quad (5)$$

The force between two MWCNTs resulting from vdW interaction potential is:

$$f(R) = -\frac{d\phi^{AB}(R)}{dR}. \quad (6)$$

Using the above ϕ^{AB} expression, the interaction force $f(R)$ could be expressed by:

$$f(R) = 1.602 \times 10^{-12} \times 705.22 \times \left(\left(\frac{3.41}{R-50+0.28}\right)^{11} - \left(\frac{3.41}{R-50+0.28}\right)^{5}\right)(\mathrm{N/A})^{\circ}. \quad (7)$$

Evidently, in all hybrid structures, MWCNTs are grown on μAl_2O_3 through base growth mode [44]. That is, one end of MWCNTs is fixed on the substrate by catalyst particles, but the other one is free. In order to emphasize the role of the length and diameter in the self-organization mechanism, we assume MWCNT as hollow homogeneous cylindrical cantilever, as reported in earlier experimental and theoretical studies [38,45]. The beam endures an attractive force from adjacent CNTs. For vertically aligned CNT arrays, the distance R between two CNTs could be approximately estimated by $R \cong 1/\sqrt{N}$, here N is the CNT area number density. The interaction forces of two adjacent CNTs are simply seen as a uniform distributed vdW force, $f(R)$, along the length (L) of the beam axis, as shown in Fig. 9a. The resulting vertically aligned CNTs are displayed in Fig. 9b.

According to Euler–Bernoulli equation, the deflection of the beam $u(x)$ at the position x is given by:

$$EI\frac{d^4u}{dx^4} = f(R) \quad (8)$$

where E is the Young's modulus of CNT and I is the second moment of its cross-section. The moment is:

$$I = \frac{\pi}{64}\left(d_o^4 - d_i^4\right) \quad (9)$$

where d_o and d_i are the outer and inner diameters of CNT, respectively [46]. As we only consider small bending deflection of the short beam (~1 μm), the shear force can be neglected. Moreover, we assume the vdW forces as constant because of the high area number density of CNTs and their small deflection angle. After integrating Eq. (8), the CNT maximum bending deflection can be expressed by:

$$u_{max}(L) = \frac{f(R)L^4}{8EI} \quad (10)$$

It is noticed that the maximum bending deflection of one CNT depends on the vdW forces, the rigidity (EI) and the length of CNT. MWCNT rigidity is proportional to the second moment of its cross-section, which is a function of the outer and inner diameters (Eq. (9)). In addition, vdW forces are related to the distance between two CNTs. Therefore, the CNT deflection is controlled by the CNT diameter, length and its area number density on the surface of the alumina sphere.

To analyze the characteristics of CNT interaction in there different hybrids, two types of CNTs are chosen for detailed discussions. CNT(25, 8) correspond to the "short-dense-homogeneous" and "six-branch" structures and CNT(40, 32) represents the "urchin-like" one, as shown in Figs. 2 and 3g, respectively. According to the obtained vdW forces depicted in Fig. 9c, the bending deflection of two CNTs with the length increase is calculated at different gaps between two CNTs (Fig. 9d).

First, it can be seen that the maximum bending deflections of both two groups of CNTs change substantially with the distance between CNTs, or CNT area number density. Smaller is the distance between two CNTs, much easier is the deflection, with higher rates. Meanwhile, when the gap between two CNTs increases from 20 to 100 Å, the deflection falls down suddenly. This phenomenon becomes more and more evident with increasing the distance. Second, for a given gap distance, CNT(40, 32) exhibits much higher resistance to the bending deflection than CNT(25, 8). This could be first seen from the fact that small diameter CNT(25, 8) losses always the stability (deflection increases rapidly) earlier than CNT(40, 32), for the same gap distance. This phenomenon is much more evident when the gap distance is smaller. The same relationship of the difference between two deflection augmentation rates and CNT gap distance has been found. The difference of the rigidities of CNTs is less important to deflection due to weak vdW forces, when the distance between two CNTs is big, as shown in Fig. 9d (gap = 100 Å, $L \sim 1$ μm). A considerable difference of the deflections of CNT(25, 8) and CNT(40, 32) is only found when CNT is long.

CNT area number density is more than 10^{15} m^{-2} in the "short-dense-homogeneous" and "six-branch" structures. This means that the gap between CNTs with diameter of 10 nm is less than 100 Å. From the Fig. 9d, we find that the CNT under the vdW forces starts having an evident deflection when the CNT length is 1 μm. However, the area number density is much lower than 10^{14} m^{-2} for CNTs in "urchin-like" hybrid structures. For instance, for CNTs with diameter of 50 nm, the gap between the CNTs will be about 5000 Å, therefore the deflection of the CNT is negligible and it will keep growing perpendicularly on the surface of alumina particle.

The analyses described above show that weak vdW forces in CNTs with a diameter about 10 nm are large enough to create clusters, when their length reach certain critical value. In our research, the value is around 1 μm for μAl_2O_3 spheres, which have diameters around 2–5 μm. However, we noticed that CNTs grown on ceramic spheres with diameters about 700 μm, would evidently crack into different bundles only when their length is more than 400 μm [14]. This is due to the substrate constituted of ceramic spheres which have smaller curvature ~10^3 whereas, in our case the curvature of alumina is nearly about 10^6.

In order to stand parallel to their neighboring CNTs, the maximum deflection of one CNT on the spherical substrate can be estimated by $u_0 \cong L\frac{d}{r_{sub}}$, where L is the CNT length, d is the gap between two CNTs, and r_{sub} is the radius of the sphere. If we consider the area number density of CNTs and u_0 as constant, a critical value of the ratio $\frac{L}{r_{sub}}$ is required to obtain bundle structures on spherical substrates. That corresponds to: $\frac{L_{01}}{L_{02}} \cong \frac{r_{sub1}}{r_{sub2}}$, where L_{01} and L_{02} are the critical lengths

of the CNTs, and r_{sub1} and r_{sub2} are the radii of the spherical particles. Finally, we find that the in our materials, the CNT crack length is 1 μm on the 2–5 μm alumina spheres, which is coherent with the 400 μm length determined by Zhang et al. for ~700 μm ceramic spheres [14].

Therefore, when the length is smaller than 1 μm (even for high area number density and small diameter ~10 nm), CNT stiffness is sufficient enough to resist to bending deflection. Finally, CNTs stand vertically on the spherical surface of μAl_2O_3, such as "short-dense-homogenous" structures (Fig. 1a). Nevertheless, when the diameter remains about 10 nm, the increasing length greatly promotes the deflection. As a result, MWCNTs agglomerate into branches, like "six-branch" structures (Fig. 1b). MWCNTs with diameters beyond 20 nm have an enhanced rigidity, which prohibits the deflection of the elongated beam. As a consequence, the most favorable structure is the "urchin-like", which has lower CNT area number density on μAl_2O_3 (Fig. 1c).

4. Conclusions

In summary, we have demonstrated that well-organized multi-scale MWCNT–μAl_2O_3 hybrid structures have been obtained using a classical CVD process by directly growing CNTs on μAl_2O_3 without any preliminary pretreatment. The CNT organization, which is strongly dependent on the diameter, length, and area number density yields to three distinct architectures: "short-dense-homogeneous", "six-branch" and "urchin-like". The influence of these parameters on the organization of the hybrid structures is described by a nano-cantilever beam model. These latter shows that the variation of the CNT diameter and length results in significant deflection differences. This model takes into account the weak van der Waals interaction forces between two CNTs which promote individual CNTs to form bundles.

Finally, MWCNTs are initially organized in "short-dense-homogenous" state for small diameter (10 nm) and have low aspect ratio (L/D = 100), then in "six-branch" for higher aspect ratio due to length increase, and last in "urchin-like" for diameter increase. Moreover, the consecutive transformations of the hybrid material let us thinking about a flowering process in nature. Ultimately, the reported multiform hybrid structures can be easily produced in large scales (see Fig. S1, Supplementary data). They are therefore promising to contribute to the enhancement of advanced multifunctional composite materials thanks to well-organized CNT dispersion and arrangement in a polymer matrix [47].

Acknowledgements

D. He gratefully acknowledges the financial support of CSC (China Scholarship Council). The authors are thankful to Mrs. F. Garnier and Dr. P. Haghi-Ashtiani for SEM and TEM characterizations.

Appendix A. Supplementary data

Supplementary data associated with this article can be found, in the online version, at doi:10.1016/j.carbon.2009.11.039.

REFERENCES

[1] Jorio A, Dresselhaus MS, Dresselhaus G. Carbon nanotubes: advanced topics in the synthesis, structure, properties and applications (topics in applied physics 111). New York, Berlin, Heidelberg: Springer-Verlag; 2008.
[2] Popov VN. Carbon nanotubes: properties and application. Mat Sci Eng R 2004;43(3):61–102.
[3] Baughman RH, Zakhidov AA, de Heer WA. Carbon nanotubes – the route toward applications. Science 2002;297(5582):787–92.
[4] Aiping Yu PR, Sun Xiaobo, Bekyarova Elena, Itkis Mikhail E, Haddon Robert C. Enhanced thermal conductivity in a hybrid graphite nanoplatelet – carbon nanotube filler for epoxy composites. Adv Mater 2008;20(24):4740–4.
[5] Yang C-K, Zhao J, Lu JP. Magnetism of transition-metal/carbon-nanotube hybrid structures. Phys Rev Lett 2003;90(25):257203.
[6] Nasibulin AG, Pikhitsa PV, Jiang H, Brown DP, Krasheninnikov AV, Anisimov AS, et al. A novel hybrid carbon material. Nat Nanotechnol 2007;2(3):156–61.
[7] Li XL, Liu YQ, Fu L, Cao LC, Wei DC, Wang Y. Efficient synthesis of carbon nanotube–nanoparticle hybrids. Adv Funct Mater 2006;16(18):2431–7.
[8] Han ZH, Yang B, Kim SH, Zachariah MR. Application of hybrid sphere/carbon nanotube particles in nanofluids. Nanotechnology 2007;18(10):105701–4.
[9] Liu L, Grunlan JC. Clay assisted dispersion of carbon nanotubes in conductive epoxy nanocomposites. Adv Funct Mater 2007;17(14):2343–8.
[10] Gournis D, Karakassides MA, Bakas T, Boukos N, Petridis D. Catalytic synthesis of carbon nanotubes on clay minerals. Carbon 2002;40(14):2641–6.
[11] Ci L, Bai J. Novel micro/nanoscale hybrid reinforcement: multiwalled carbon nanotubes on SiC particles. Adv Mater 2004;16(22):2021–4.
[12] Thostenson ET, Li WZ, Wang DZ, Ren ZF, Chou TW. Carbon nanotube/carbon fiber hybrid multiscale composites. J Appl Phys 2002;91(9):6034–7.
[13] Huang S. Growing carbon nanotubes on patterned submicron-size SiO_2 spheres. Carbon 2003;41(12):2347–52.
[14] Zhang Q, Huang J-Q, Zhao M-Q, Qian W-Z, Wang Y, Wei F. Radial growth of vertically aligned carbon nanotube arrays from ethylene on ceramic spheres. Carbon 2008;46(8):1152–8.
[15] Zhang Q, Huang JQ, Wei F, Xu GH, Wang Y, Qian WZ, et al. Large scale production of carbon nanotube arrays on the sphere surface from liquefied petroleum gas at low cost. Chin Sci Bull 2007;52(21):2896–902.
[16] Xiang R, Luo G, Qian W, Wang Y, Wei F, Li Q. Large area growth of aligned CNT arrays on spheres: towards large scale and continuous production. Chem Vapor Deposition 2007;13(10):533–6.
[17] Philippe R, Caussat B, Falqui A, Kihn Y, Kalck P, Bordere S, et al. An original growth mode of MWCNTs on alumina supported iron catalysts. J Catal 2009;263(2):345–58.
[18] Yamamoto N, John Hart A, Garcia EJ, Wicks SS, Duong HM, Slocum AH, et al. High-yield growth and morphology control of aligned carbon nanotubes on ceramic fibers for multifunctional enhancement of structural composites. Carbon 2009;47(3):551–60.
[19] Ci LJ, Zhao ZG, Bai JB. Direct growth of carbon nanotubes on the surface of ceramic fibers. Carbon 2005;43(4):883–6.
[20] Zhao ZG, Ci LJ, Cheng HM, Bai JB. The growth of multi-walled carbon nanotubes with different morphologies on carbon fibers. Carbon 2005;43(3):663–5.
[21] Wei BQ, Vajtai R, Jung Y, Ward J, Zhang R, Ramanath G, et al. Assembly of highly organized carbon nanotube architectures by chemical vapor deposition. Chem Mat 2003;15(8):1598–606.

[22] Bae EJ, Choi WB, Jeong KS, Chu JU, Park G-S, Song S, et al. Selective growth of carbon nanotubes on pre-patterned porous anodic aluminum oxide. Adv Mater 2002;14(4):277–9.
[23] Hata K, Futaba DN, Mizuno K, Namai T, Yumura M, Iijima S. Water-assisted highly efficient synthesis of impurity-free single-walled carbon nanotubes. Science 2004;306(5700):1362–4.
[24] Sohn JI, Lee S, Song Y-H, Choi S-Y, Cho K-I, Nam K-S. Patterned selective growth of carbon nanotubes and large field emission from vertically well-aligned carbon nanotube field emitter arrays. Appl Phys Lett 2001;78(7):901–3.
[25] Hart AJ, Slocum AH. Rapid growth and flow-mediated nucleation of millimeter-scale aligned carbon nanotube structures from a thin-film catalyst. J Phys Chem B 2006;110(16):8250–7.
[26] Ren ZF, Huang ZP, Xu JW, Wang JH, Bush P, Siegal MP, et al. Synthesis of large arrays of well-aligned carbon nanotubes on glass. Science 1998;282(5391):1105–7.
[27] Kim K-E, Kim K-J, Jung WS, Bae SY, Park J, Choi J, et al. Investigation on the temperature-dependent growth rate of carbon nanotubes using chemical vapor deposition of ferrocene and acetylene. Chem Phys Lett 2005;401(4–6):459–64.
[28] Hernadi K, Fonseca A, Nagy JB, Siska A, Kiricsi I. Production of nanotubes by the catalytic decomposition of different carbon-containing compounds. Appl Catal A: Gen 2000;199(2):245–55.
[29] Zhang G, Mann D, Zhang L, Javey A, Li Y, Yenilmez E, et al. Ultra-high-yield growth of vertical single-walled carbon nanotubes: hidden roles of hydrogen and oxygen. Proc Natl Acad Sci USA 2005;102(45):16141–5.
[30] Wasel W, Kuwana K, Reilly PTA, Saito K. Experimental characterization of the role of hydrogen in CVD synthesis of MWCNTs. Carbon 2007;45(4):833–8.
[31] Nessim GD, Hart AJ, Kim JS, Acquaviva D, Oh J, Morgan CD, et al. Tuning of vertically-aligned carbon nanotube diameter and areal density through catalyst pre-treatment. Nano Lett 2008;8(11):3587–93.
[32] Endo M, Kim YA, Hayashi T, Fukai Y, Oshida K, Terrones M, et al. Structural characterization of cup-stacked-type nanofibers with an entirely hollow core. Appl Phys Lett 2002;80(7):1267–9.
[33] Chráska P, Dubsky J, Neufuss K, Písacka J. Alumina-base plasma-sprayed materials part I: phase stability of alumina and alumina–chromia. J Ther Spray Technol 1997;6(3):320–6.
[34] Kittaka S, Morimto T. Spherical particles and their surface properties. III. Formation of spherical particles of metal oxides by O_2–H_2 flame fusion. Bull Chem Soc Jpn 1981;54(10):2882–5.
[35] Porto SPS, Krishnan RS. Raman effect of corundum. J Chem Phys 1967;47(3):1009–12.
[36] Girifalco LA, Hodak M, Lee RS. Carbon nanotubes, buckyballs, ropes, and a universal graphitic potential. Phys Rev B 2000;62(19):13104.
[37] Henrard L, Hernandez E, Bernier P, Rubio A. van der Waals interaction in nanotube bundles: consequences on vibrational modes. Phys Rev B 1999;60(12):R8521–4.
[38] Kis A, Csanyi G, Salvetat JP, Lee T-N, Couteau E, Kulik AJ, et al. Reinforcement of single-walled carbon nanotube bundles by intertube bridging. Nat Mater 2004;3(3):153–7.
[39] Buehler MJ. Mesoscale modeling of mechanics of carbon nanotubes: self-assembly, self-folding, and fracture. J Mater Res 2006;21(11):2855–69.
[40] Fan SS, Chapline MG, Franklin NR, Tombler TW, Cassell AM, Dai HJ. Self-oriented regular arrays of carbon nanotubes and their field emission properties. Science 1999;283(5401):512–4.
[41] Dai HJ. Carbon nanotubes: synthesis, integration, and properties. Acc Chem Res 2002;35(12):1035–44.
[42] Sun C-H, Yin L-C, Li F, Lu G-Q, Cheng H-M. van der Waals interactions between two parallel infinitely long single-walled nanotubes. Chem Phys Lett 2005;403(4–6):343–6.
[43] Sun C-H, Lu G-Q, Cheng H-M. Simple approach to estimating the van der Waals interaction between carbon nanotubes. Phys Rev B 2006;73(19):195414–5.
[44] Baker RTK. Catalytic growth of carbon filaments. Carbon 1989;27(3):315–23.
[45] Wong EW, Sheehan PE, Lieber CM. Nanobeam mechanics: elasticity, strength, and toughness of nanorods and nanotubes. Science 1997;277(5334):1971–5.
[46] Gere JM, Timoshenko SP. Mechanics of materials. Boston: PWS–Kent; 1984.
[47] Bozlar M, He D, Bai J, Chalopin Y, Mingo N, Volz S. Advanced carbon nanotube microarchitectures for enhanced thermal conduction at ultra-low mass fraction in polymer composites. Adv Mater 2009. doi: 10.1002/adma.200901955.